Electronic Supplementary Information

Cobalt and nickel compounds with pentadienyl and edge-bridged pentadienyl ligands revisited

Matthias Reiners, Ann Christin Fecker, Dirk Baabe, Matthias Freytag, Peter G. Jones, Marc D. Walter*

Institut für Anorganische und Analytische Chemie, Technische Universität Braunschweig, Hagenring 30, 38106 Braunschweig, Germany

Table of contents

1. Crystallographic details

Hydrogen atom treatment:

Hydrogen atoms of the pentadienide groups were refined freely (see below for individual details), but in some cases with a C-H distance restraint (SADI). Methyl groups were refined as idealised rigid groups allowed to rotate but not tip. Other hydrogens were included using a riding model starting from calculated positions.

Special refinement details:

Complexes 1, 2, 3, 3', 4: The hydrogen atoms at C1, C3 and C5 were refined freely

Complex 4: The structure was refined as a non-merohedral twin using the "HKLF 5" method; relative twin volumes refined to 0.524, 0.476(2). Two consequences of this method are (a) that the number of reflections becomes ill-defined (because of overlapping reflections and the "extra" reflections from component 2) and (b) *R*(int) becomes meaningless. At the end of the refinement, one significant peak of residual electron density (2 e/Å^3) remained. This was related to the Ni atom by the non-space-group operator *x*, 0.5-*y*, *z*, and may be caused by imperfections in the detwinning process. Nonetheless we believe the structure determination to be reliable.

Complex 5: The ring hydrogen atoms at C1,2,3,4,5; 9,10,11,12,13; 17,18,19,20,21; 25,26,27,28,29 were refined freely. Three large difference peaks were refined as carbon atoms and corresponded to a hexane molecule over an inversion center. Although these three atoms refined well, further peaks indicated alternative positions for the solvent atoms, and these could not be refined satisfactorily as disorder sites. For this reason, the routine SQUEEZE (part of the PLATON program suite [1]) was used to remove mathematically the effects of the solvent. A solvent content of one hexane per cell was assumed when deriving the molar mass and related parameters.

Complexes 7, 8, 11-R and 12-R: The hydrogen atoms at C1-C5 were refined freely (as were, for **11-Et** and **12-Et**, the corresponding atoms in the second independent molecule).

Complex 11-Me: The sample was not a pure enantiomer and crystallizes only by chance in a chiral (Sohncke) space group.

Complex 12-Et: The crystal was a non-merohedral twin by 180° rotation about **a***. The structure was refined using the "HKLF 5" method, with relative volume 0.26291(9) for the smaller component. Because of the overlapped reflections and the reflections from component 2, reflection numbers are not well-defined. Equivalent reflections are merged during the untwining procedures and R(int) is therefore meaningless. Some scattered difference peaks of 0.5 to 1 e/A**3 could not be interpreted and may be caused by unidentified disorder or residual twinning errors.

Table S1. Crystallographic data.

Compound reference	**1**	**2**	**3**	**3'**	**4**	**5**	**7**	**8**
Chemical formula	$C_{26}H_{46}Co$	$C_{18}H_{30}NiO_2$	$C_{26}H_{46}Ni$	$C_{26}H_{46}Ni$	$C_{26}H_{46}Ni_2$	$C_{35}H_{51}Co_2$	$C_{16}H_{22}Ni$	$C_{16}H_{22}Ni$
Formula Mass	417.56	337.13	417.34	417.34	476.05	589.61	273.05	273.05
Crystal system	monoclinic	monoclinic	monoclinic	monoclinic	monoclinic	triclinic	monoclinic	monoclinic
a/Å	12.6850(2)	9.5194(3)	12.5912(3)	9.8802(4)	18.4581(6)	10.5797(6)	5.7057(2)	11.3689(4)
b/Å	6.8084(2)	6.3057(2)	6.8753(2)	12.3943(5)	7.2552(2)	11.2717(6)	17.2621(3)	7.4997(3)
c/Å	13.8159(3)	29.9709(8)	13.9099(3)	10.6434(5)	18.2568(6)	13.5645(4)	7.2845(2)	15.3724(6)
α/°	90	90	90	90	90	79.841(4)°	90	90
β/°	93.061(2)	93.516(3)	94.055(2)	107.309(5)	90.101(3)	89.373(4)°	108.290(3)	90.765(4)°
γ/°	90	90	90	90	90	70.997(5)°	90	90
Unit cell volume/Å^3	1191.50	1795.66	1201.14	1244.24	2444.91	1503.57	681.22	1310.58
Temperature/K	100(2)	100(2)	100(2)	100(2)	100(2)	100(2)	100(2)	100(2)
Space group	$P2_1/n$	$P2_1/n$	$P2_1/n$	$P2_1$/n	$C2/c$	$P\bar{1}$	$P2_1/n$	$C2/c$
No. of formula units per unit cell, *Z*	2	4	2	2	4	2	2	4
Radiation type	Mo Kα	Mo Kα	Mo Kα	Cu Kα	Cu Kα	Mo Kα	Cu Kα	Cu Kα
Absorption coefficient, *μ*/mm^{-1}	0.73	1.08	0.82	1.15	1.95	1.13	1.33	1.90
$2\theta_{max}$	62	60	62	152	152	60	152	152
No. of reflections measured	99589	119616	61694	25200	2682	79886	12868	10438
No. of independent reflections	3651	5230	3688	2599	2682	8634	1423	1365
R_{int}	0.038	0.048	0.045	0.044	-	0.071	0.034	0.053
No. of parameters	150	218	150	150	154	395	101	99
Final R_1 values ($I > 2\sigma(I)$)	0.0259	0.0312	0.0271	0.0321	0.0374	0.0362	0.0273	0.0315
Final $wR(F^2)$ values ($I > 2\sigma(I)$)	0.0656	0.0649	0.0624	0.0841	0.1011	0.0754	0.0718	0.0827
Final R_1 values (all data)	0.0301	0.0357	0.0346	0.0398	0.0390	0.0504	0.0284	0.0340
Final $wR(F^2)$ values (all data)	0.0677	0.0662	0.0658	0.0911	0.1024	0.0805	0.0730	0.0851
Goodness of fit on F^2	1.03	1.20	1.07	1.07	1.04	1.03	1.06	1.05
Flack parameter	-	-	-	-	-	-	-	-
$\Delta\rho$ / e Å^{-3}	0.49/-0.23	0.42/-0.53	0.43/-0.30	0.26/-0.29	1.99/-0.34	0.51/-0.37	0.24/-0.53	0.35/-0.36
CCDC	1946601	1946602	1946604	1948879	1946603	1946605	1946606	1946607

Table S1 (continued). Crystallographic data.

Compound reference	**11-Me**	**11-Et**	**12-Me**	**12-Et**
Chemical formula	$C_{17}H_{36}CoP_3$	$C_{21}H_{44}CoP_3$	$C_{15}H_{27}CoOP_2$	$C_{19}H_{35}CoOP_2$
Formula Mass	392.30	448.40	344.24	400.34
Crystal system	orthorhombic	monoclinic	monoclinic	triclinic
a/Å	9.0730(2)	31.5080(11)	12.62179(14)	8.5186(6)
b/Å	13.9554(4)	9.9790(3)	11.28232(12)	13.4821(10)
c/Å	16.1582(5)	15.5608(6)	12.20384(14)	18.8157(10)
α/°	90	90	90	91.694(5)
β/°	90	103.412(4)	91.5925(5)	91.213(6)
γ/°	90	90	90	106.619(7)
Unit cell volume/Å^3	2045.91	4759.2	1737.19	2068.8
Temperature/K	100(2)	100(2)	100(2)	100(2)
Space group	$P2_12_12_1$	*Cc*	$P2_1/c$	$P\bar{1}$
No. of formula units per unit cell, *Z*	4	8	4	4
Radiation type	Cu Kα	Mo Kα	Cu Kα	Mo Kα
Absorption coefficient, *μ*/mm^{-1}	8.7	0.93	9.4	0.99
$2\theta_{max}$	152	60	152	60
No. of reflections measured	42461	69264	35027	14551
No. of independent reflections	4269	13506	3616	14551
R_{int}	0.088	0.058	0.069	-
No. of parameters	217	505	196	464
Final R_1 values ($I > 2\sigma(I)$)	0.0468	0.0355	0.0359	0.0413
Final $wR(F^2)$ values ($I > 2\sigma(I)$)	0.1014	0.0648	0.0935	0.0942
Final R_1 values (all data)	0.0479	0.0442	0.0370	0.0687
Final $wR(F^2)$ values (all data)	0.1021	0.0690	0.0943	0.0990
Goodness of fit on F^2	1.07	1.05	1.05	0.92
Flack parameter	-0.006(5)	-0.008(4)		-
$\Delta\rho$ / e Å^{-3}	0.38/-0.45	0.44/-0.33	0.47/-0.63	0.90/-0.59
CCDC	1946608	1946609	1946610	1946611

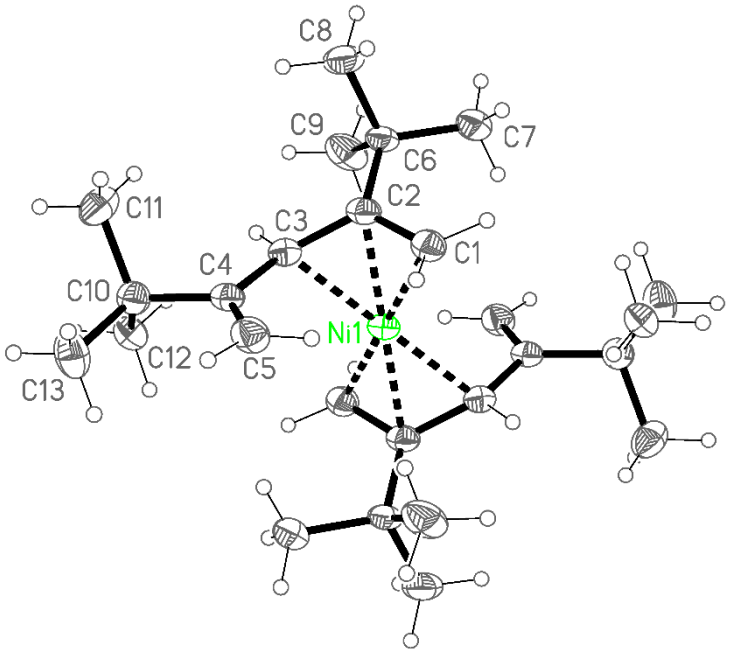

Figure S1. Molecular structure of the second polymorph **3'** of compound **3**. The molecules of **3** and **3'** are closely similar, although the butyl group C7/8/9 displays slightly different orientations.

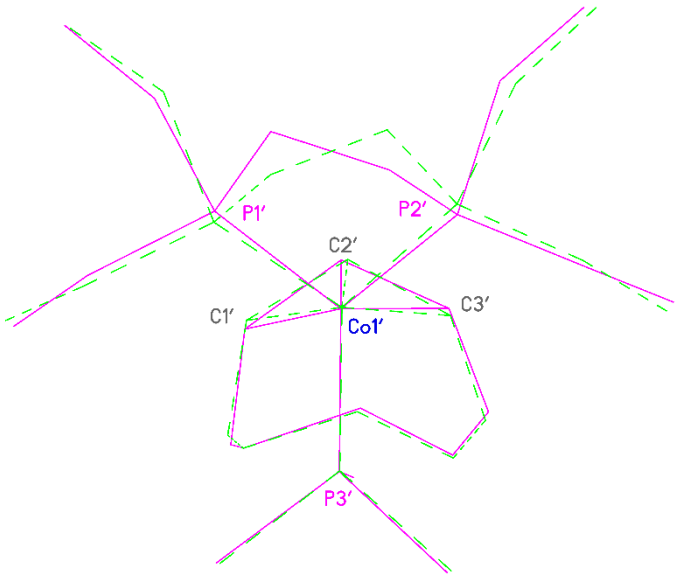

Figure S2. Overlay of the molecular structures of the two independent molecules for **11-Et**.

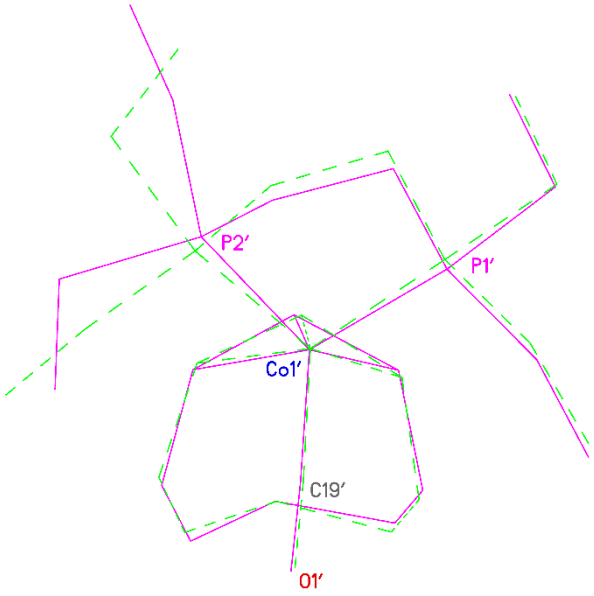

Figure S3. Overlay of the molecular structures of the two independent molecules for **12-Et**.

2. NMR Spectra

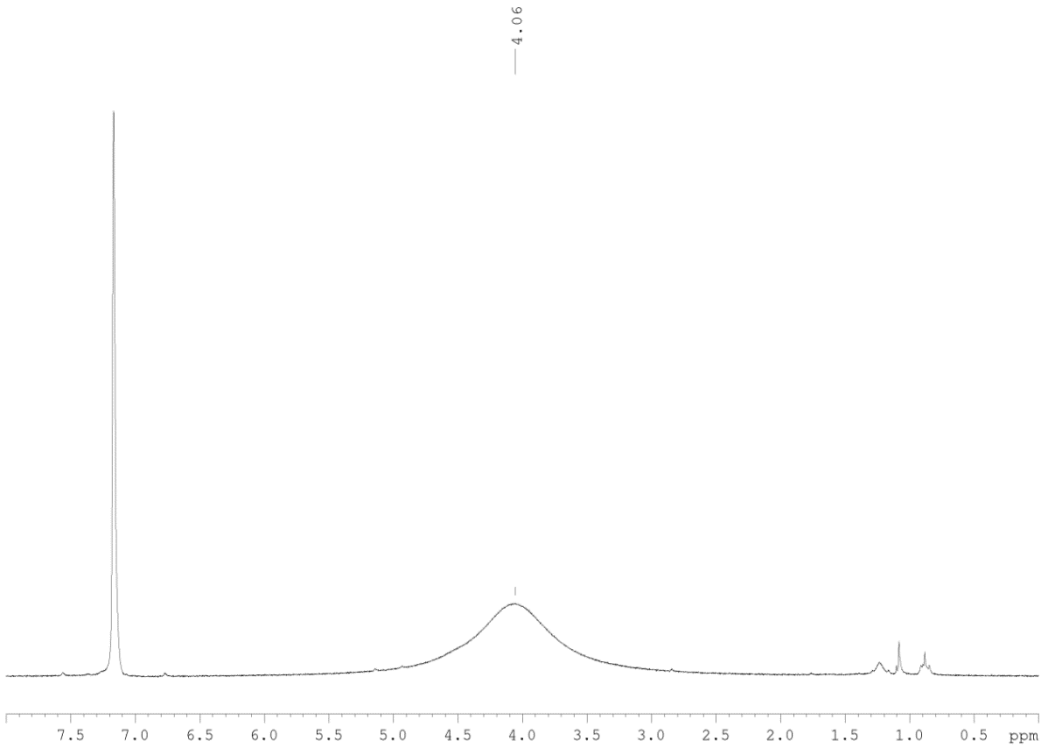

Figure S4. ^{1}H NMR spectrum (C_6D_6, 298 K) for **1**.

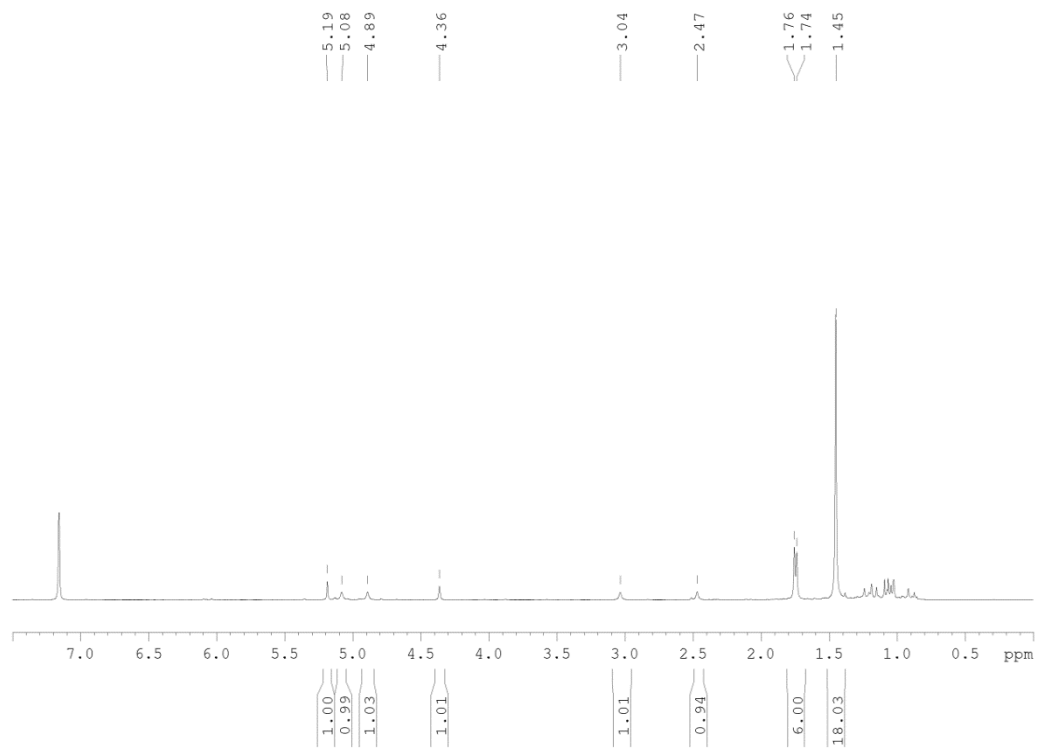

Figure S5. ^{1}H NMR spectrum (C_6D_6, 298 K) for **2**.

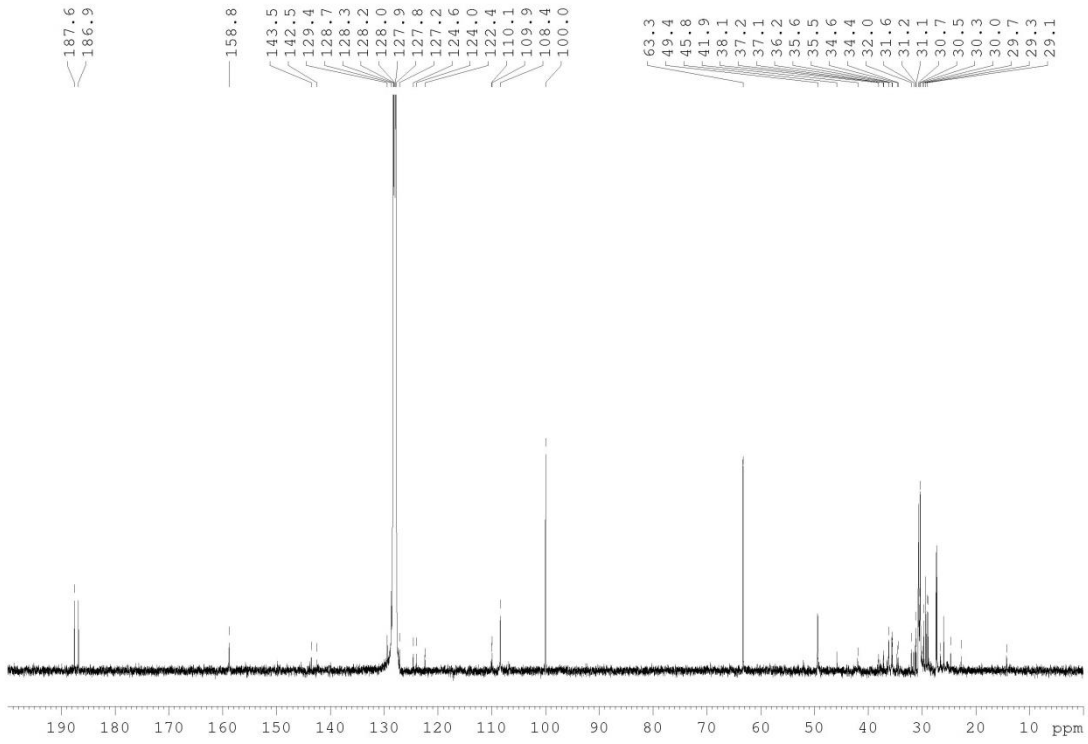

Figure S6. $^{13}C\{^{1}H\}$ NMR spectrum (C_6D_6, 298 K) for **2**.

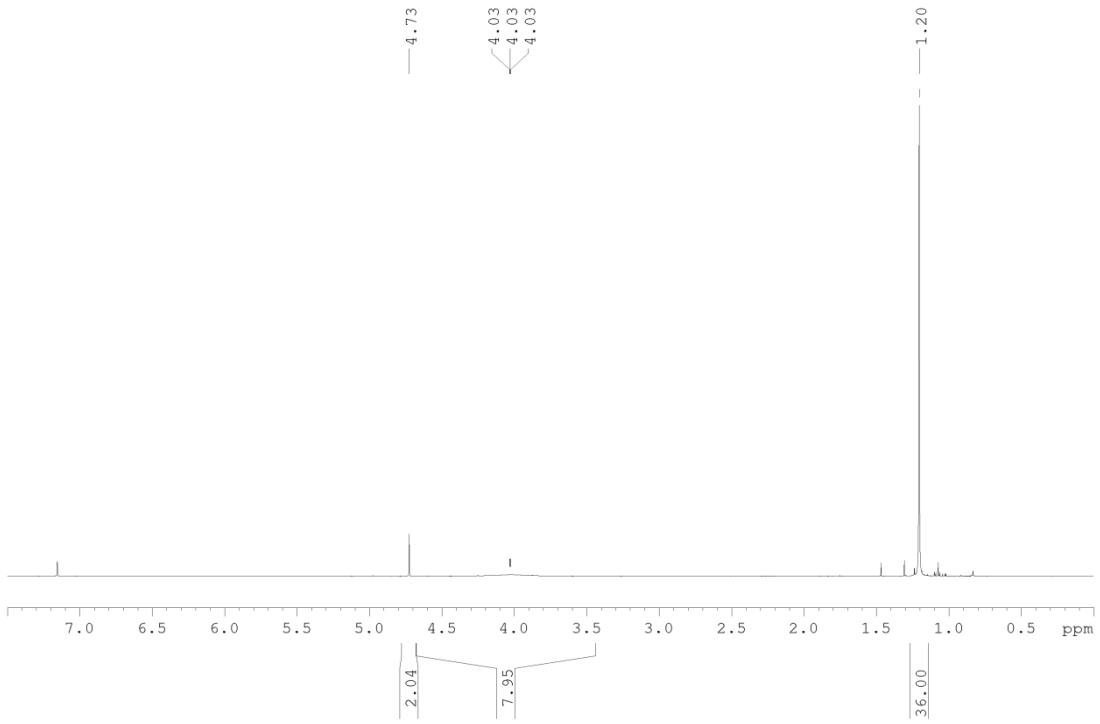

Figure S7. ^{1}H NMR spectrum (C_6D_6, 298 K) for **3**.

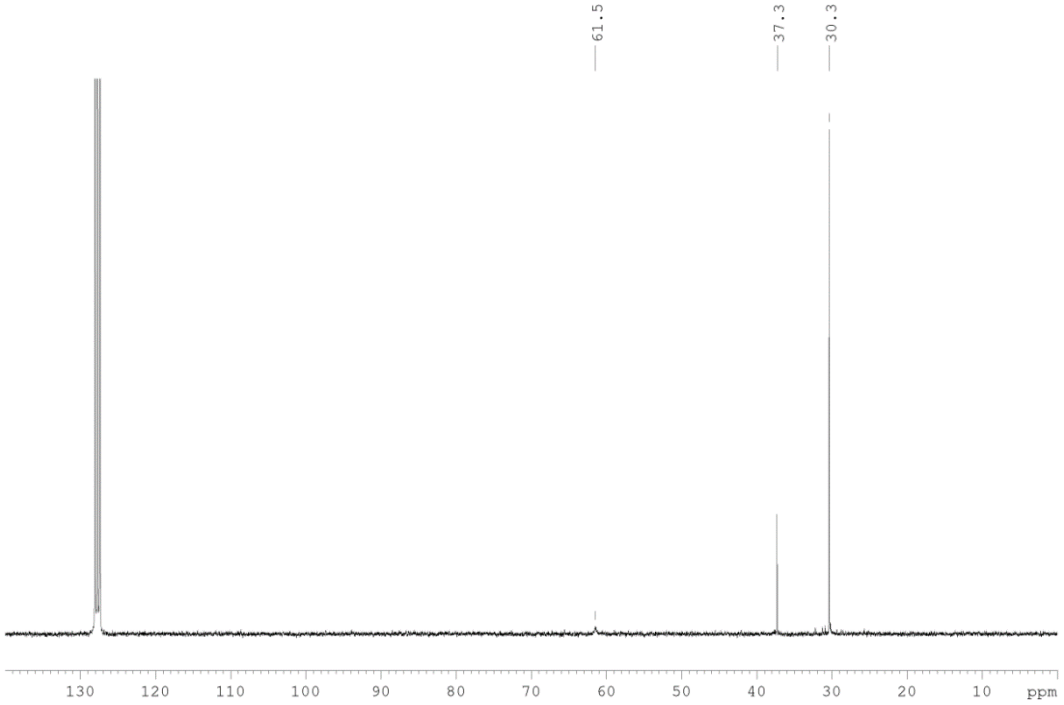

Figure S8. $^{13}C\{^{1}H\}$ NMR spectrum (C_6D_6, 298 K) of **3**.

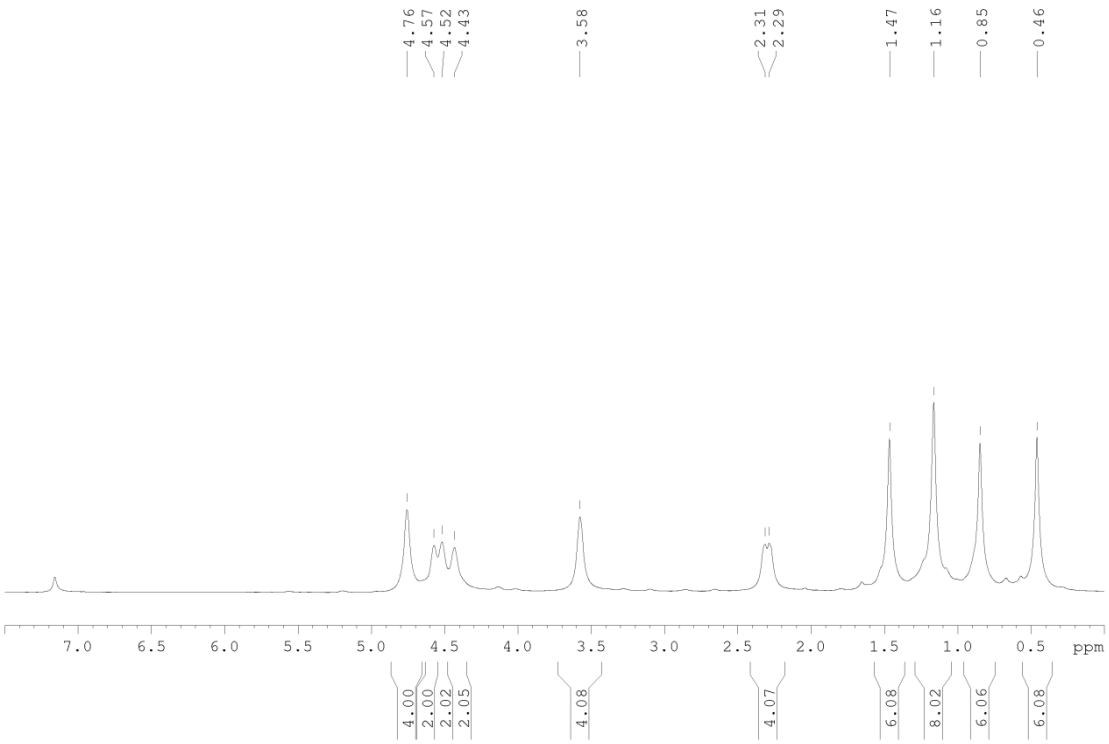

Figure S9. ^{1}H NMR spectrum (C_6D_6, 298 K) for **5**.

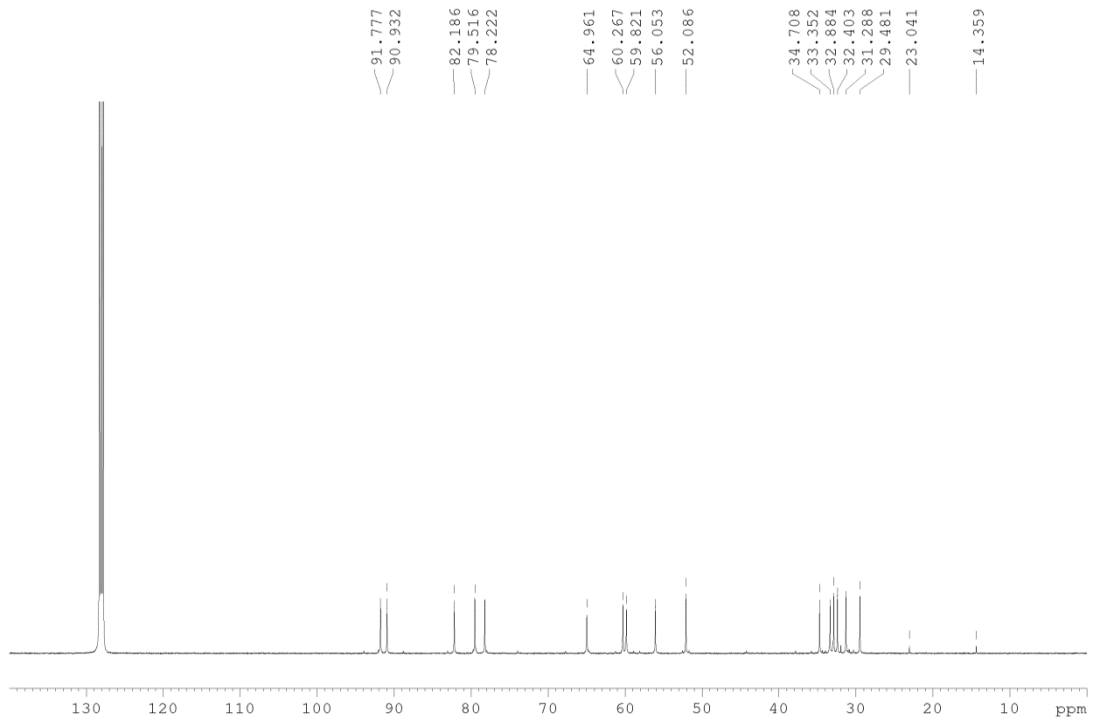

Figure S10. $^{13}C\{^{1}H\}$ NMR spectrum (C_6D_6, 298 K) for **5.**

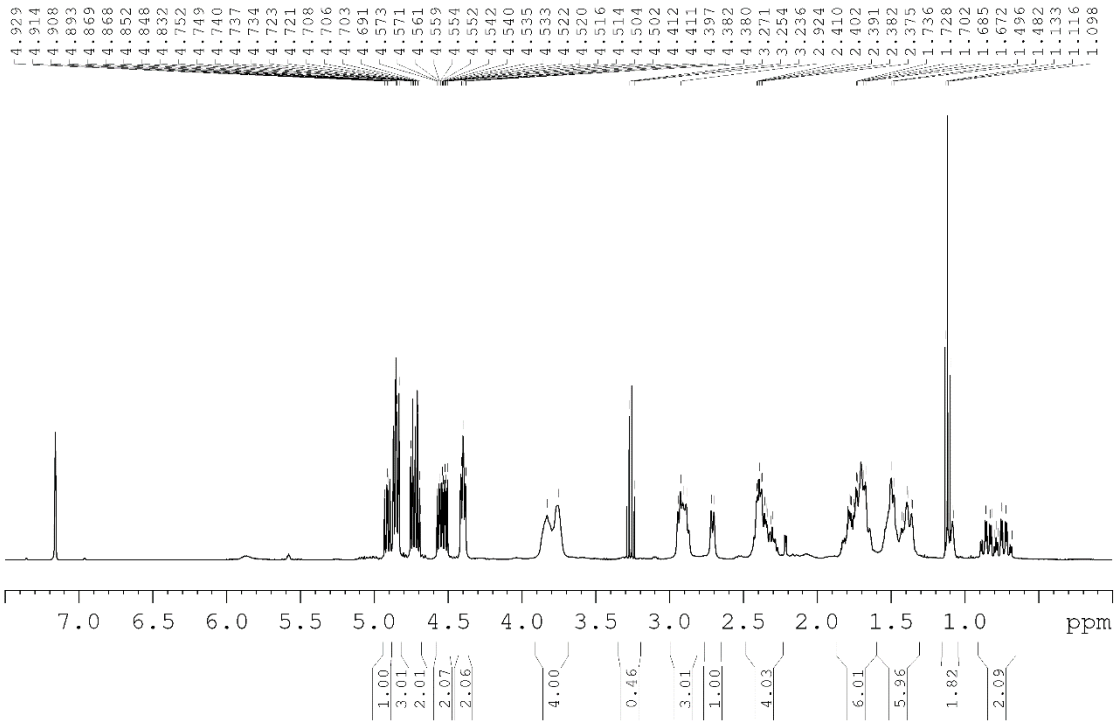

Figure S11. ^{1}H NMR spectrum (C_6D_6, 298 K) for **6**.

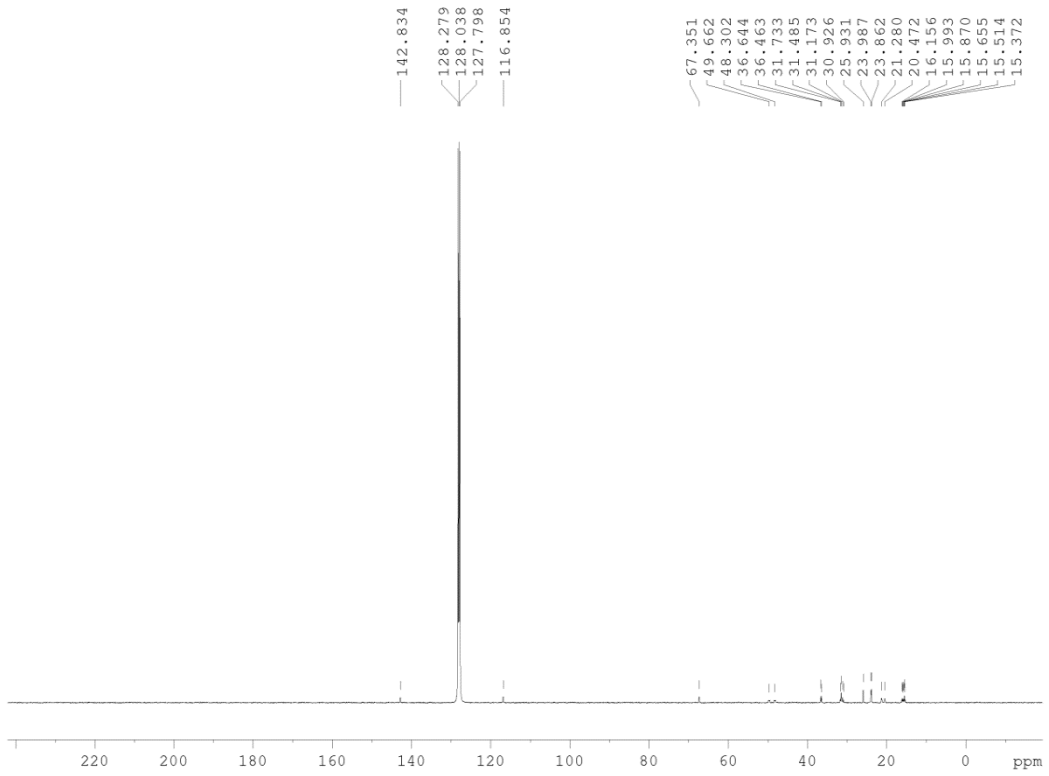

Figure S12. $^{13}C\{1H\}$ NMR spectrum (C_6D_6, 298 K) for **6**.

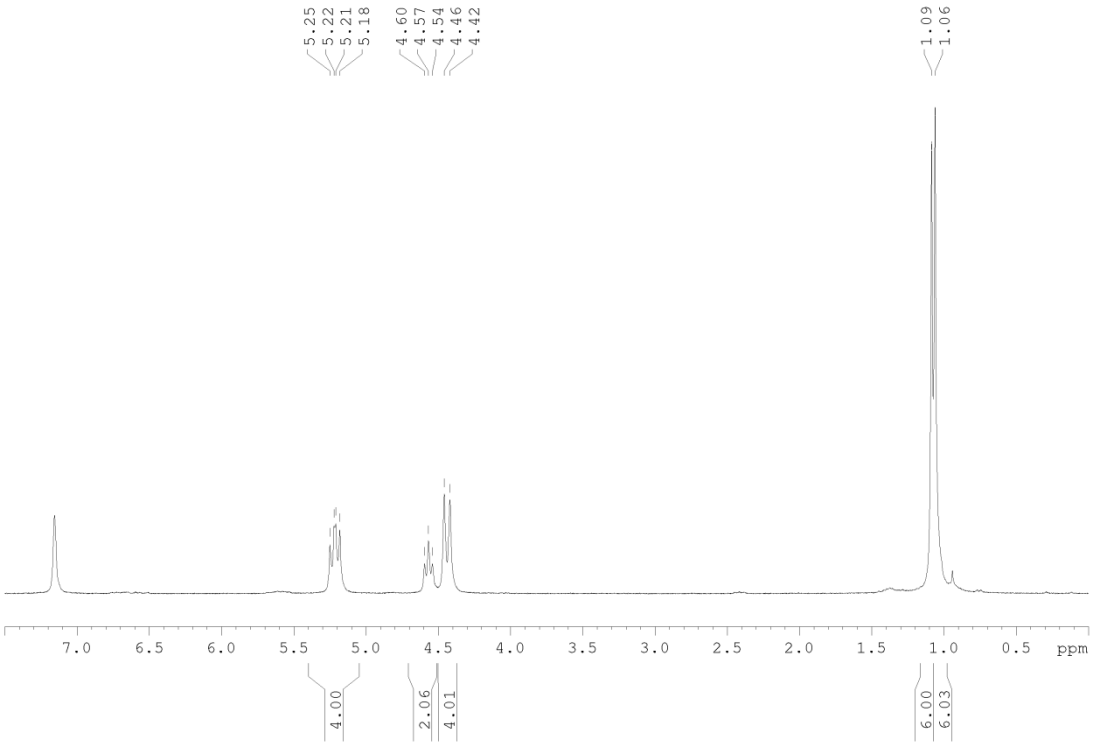

Figure S13. ^{1}H NMR spectrum (C_6D_6, 298 K) of **7**.

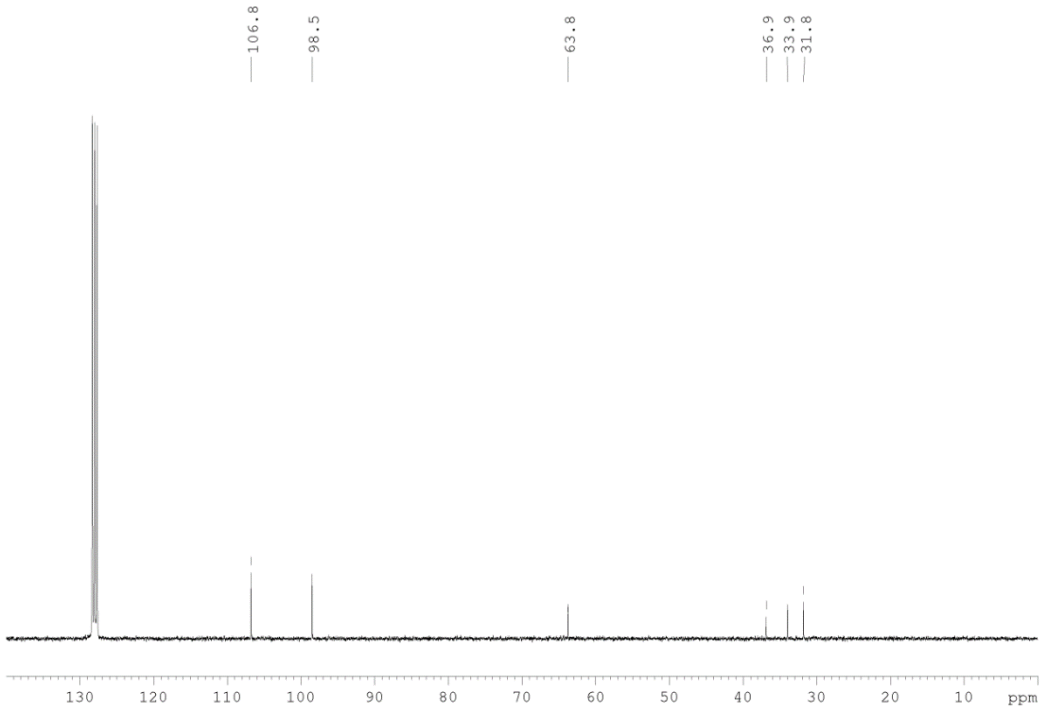

Figure S14. $^{13}C\{^{1}H\}$ NMR (C_6D_6, 298 K) for **7**.

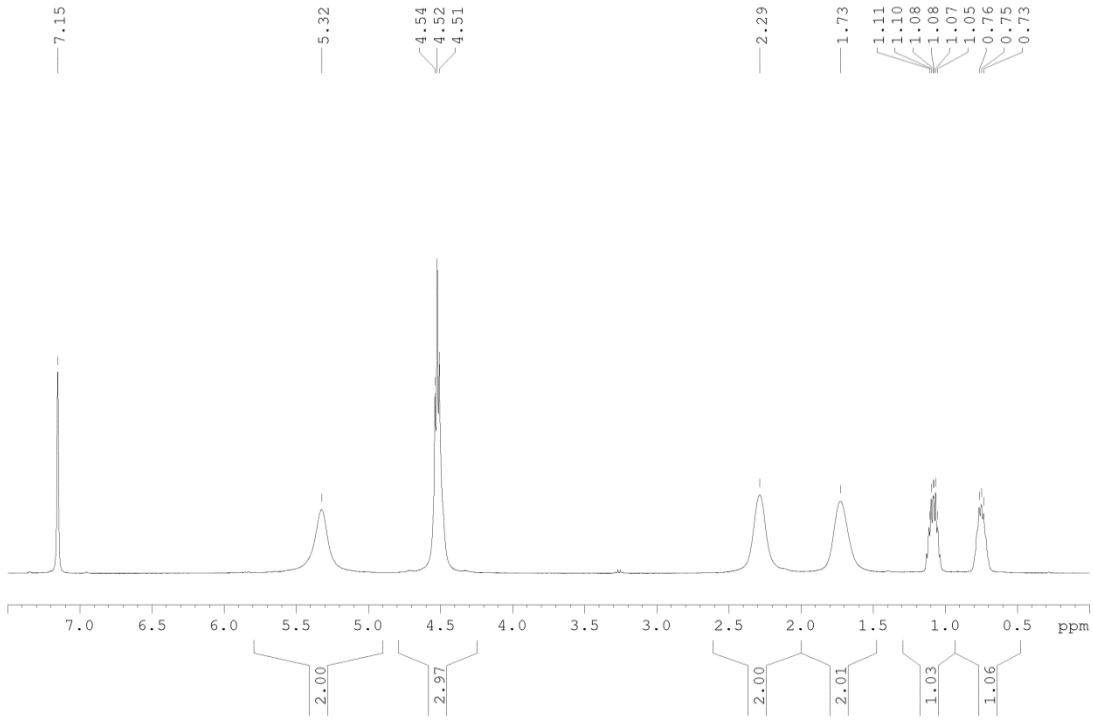

Figure S15. ^{1}H NMR spectrum (C_6D_6, 298 K) of **8**.

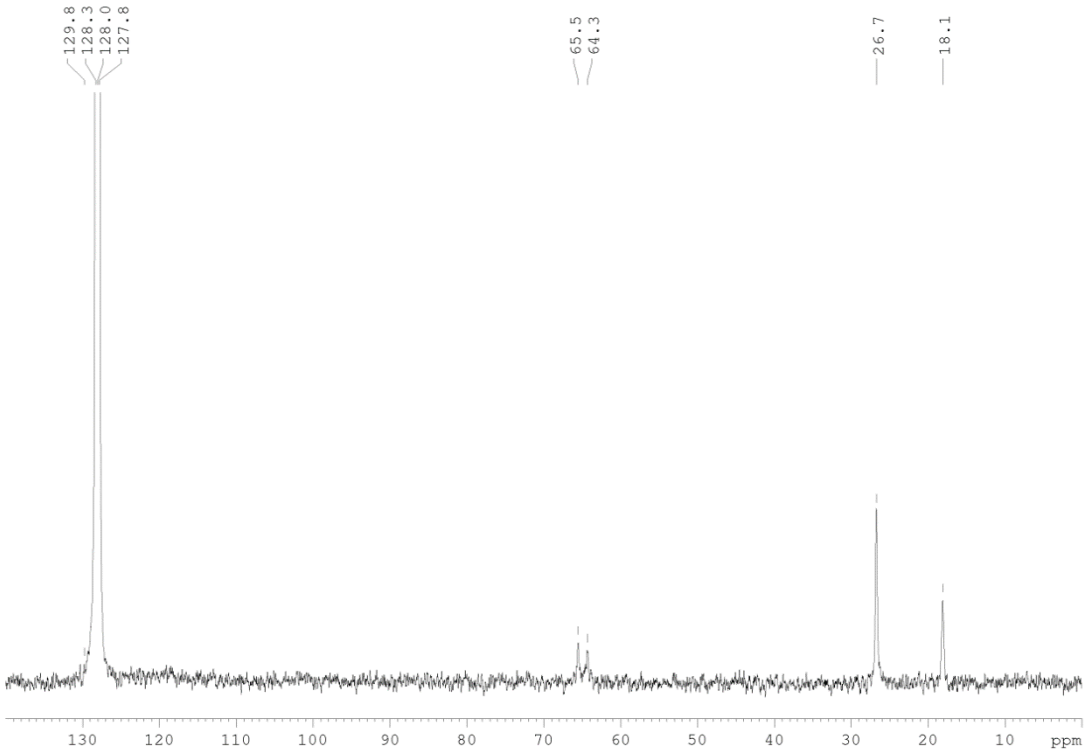

Figure S16. $^{13}C\{^{1}H\}$ NMR spectrum (C_6D_6, 298 K) for **8**.

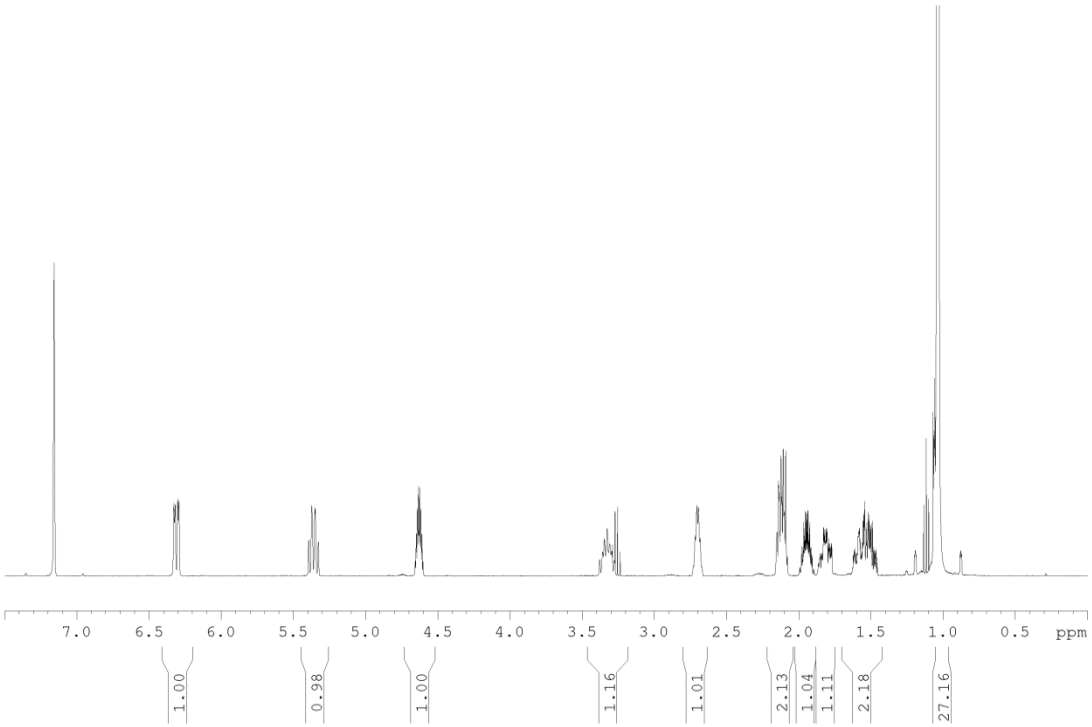

Figure S17. ^{1}H NMR spectrum (C_6D_6, 298 K) for **9**.

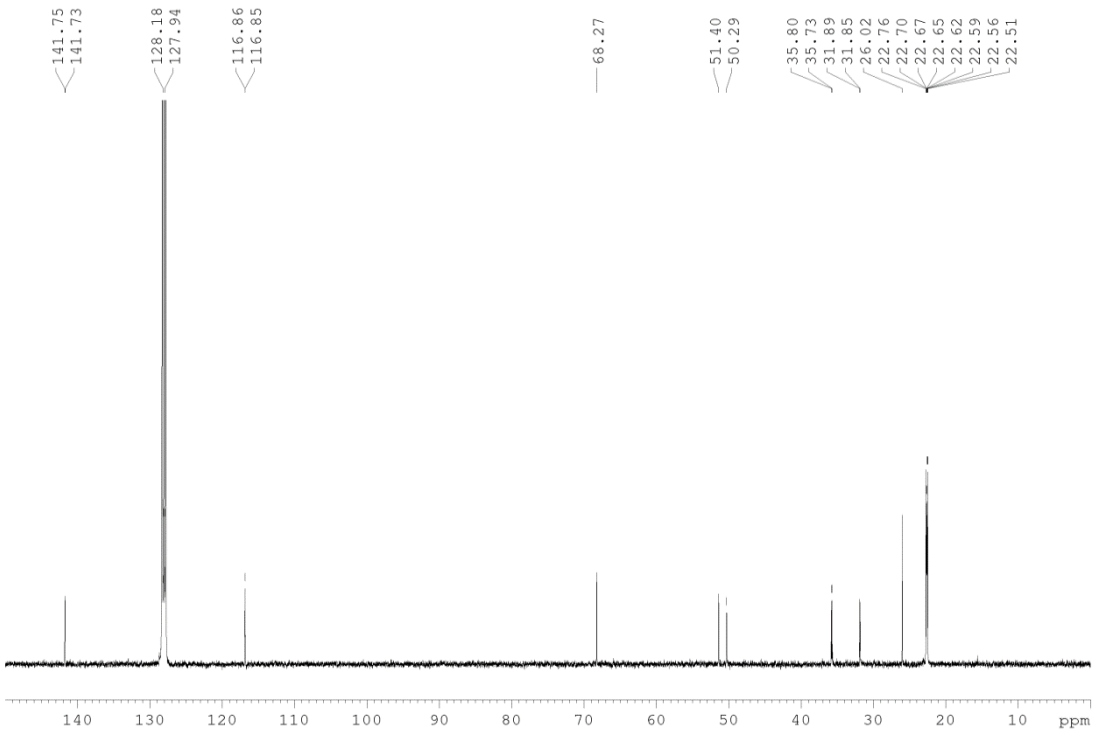

Figure S18. $^{13}C\{^{1}H\}$ NMR spectrum (C_6D_6, 298 K) for **9**.

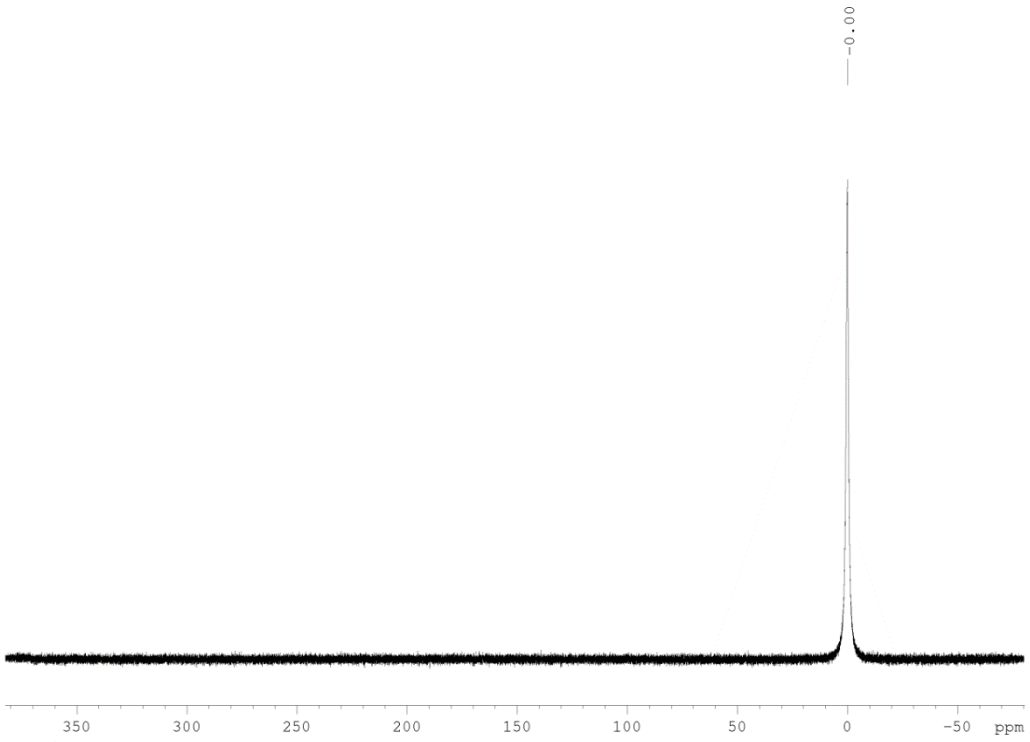

Figure S19. $^{31}P\{^{1}H\}$ NMR spectrum (C_6D_6, 298 K) for **9**.

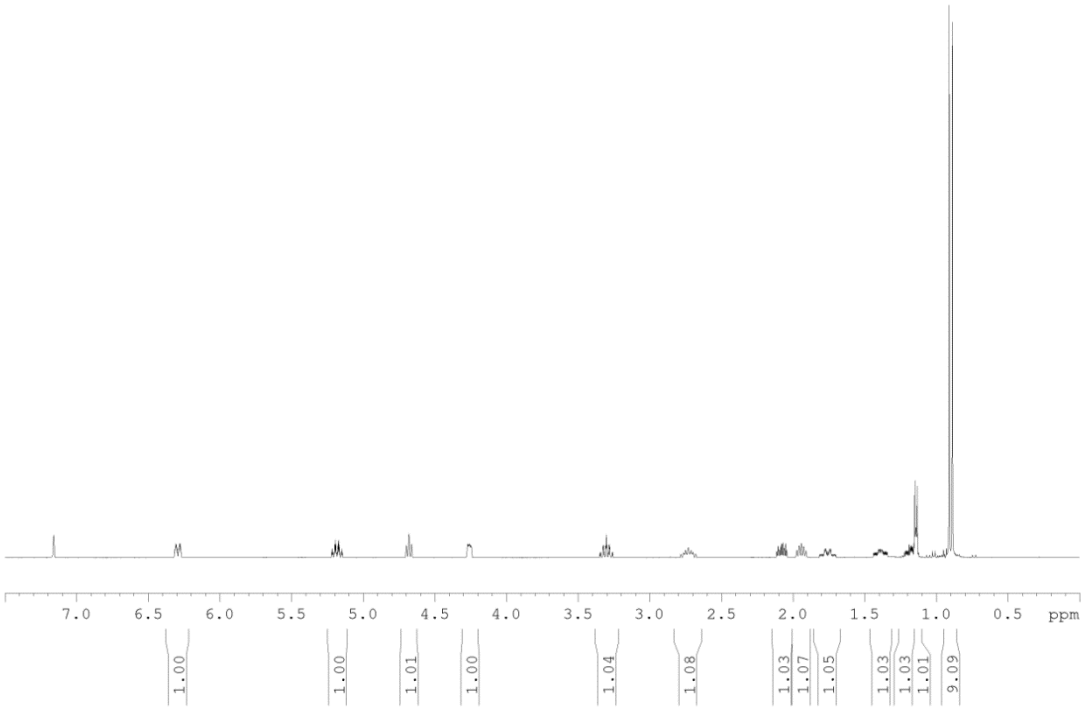

Figure S20. ^{1}H NMR spectrum (C_6D_6, 298 K) for **10**.

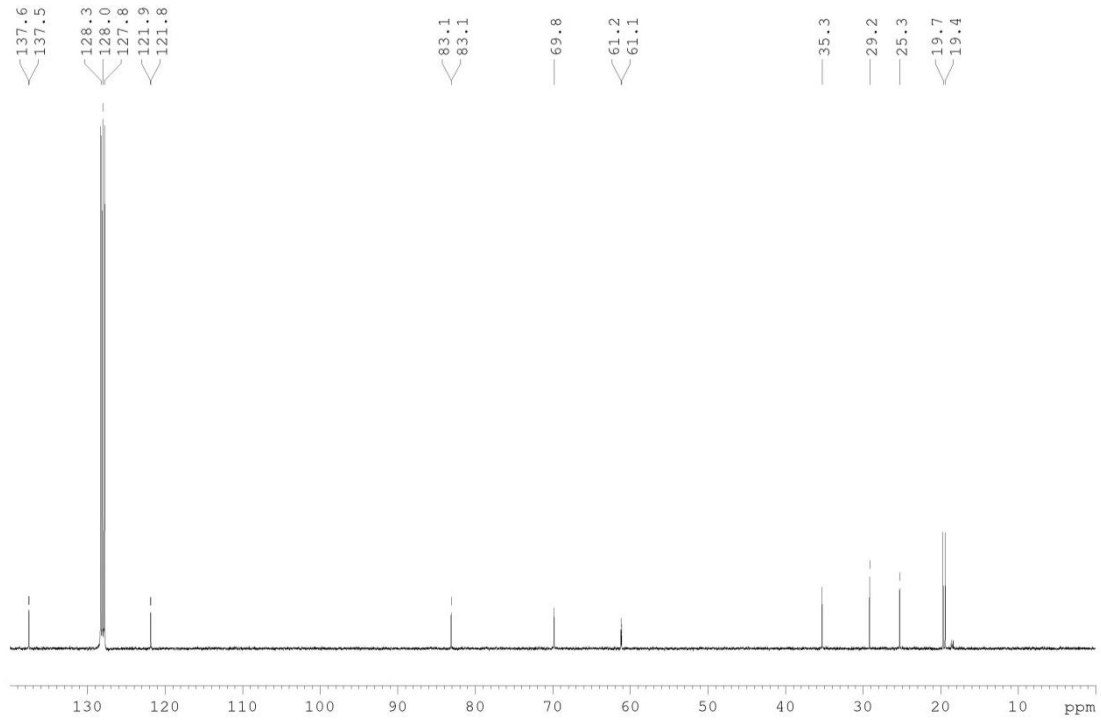

Figure S21. ^{13}C{^{1}H} NMR spectrum (C_6D_6, 298 K) for **10**.

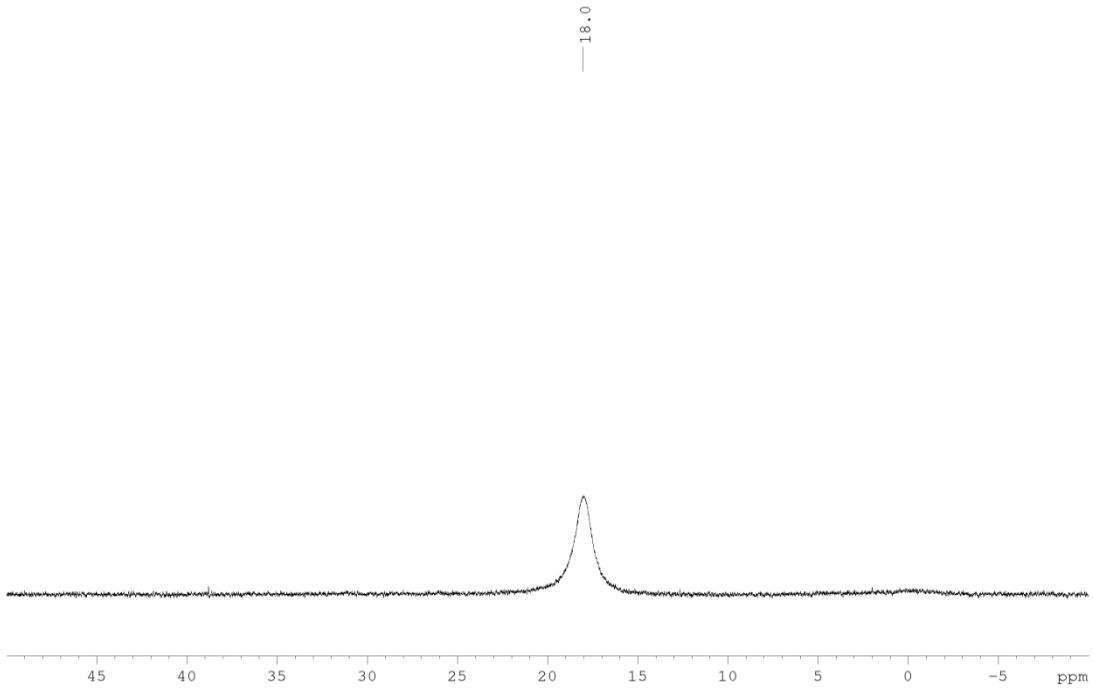

Figure S22. $^{31}P\{^{1}H\}$ NMR spectrum (C_6D_6, 298 K) for **10**.

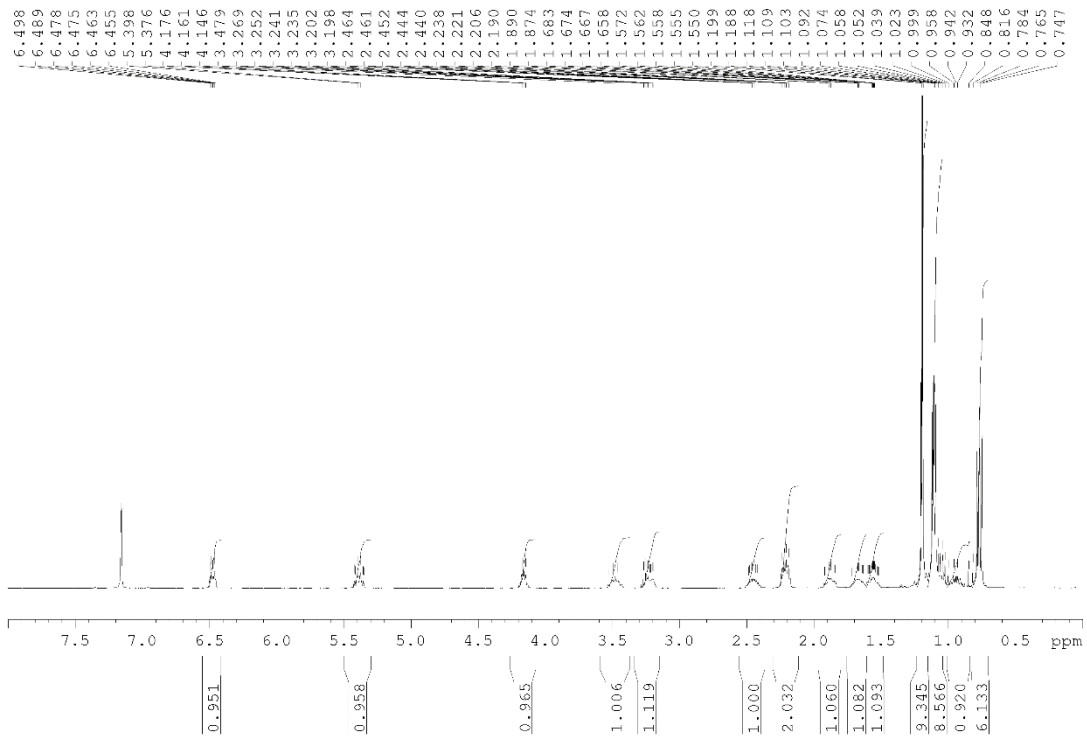

Figure S23. ^{1}H NMR spectrum (C_6D_6, 298 K) for **11-Me**.

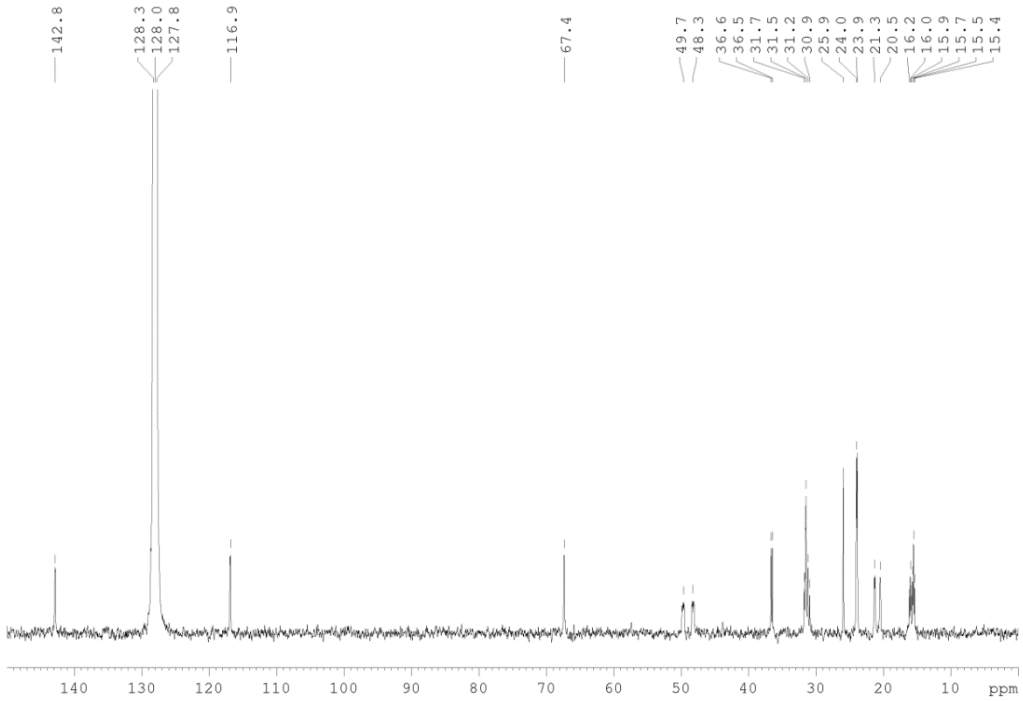

Figure S24. $^{13}C\{^{1}H\}$ NMR spectrum (C_6D_6, 298 K) for **11-Me**.

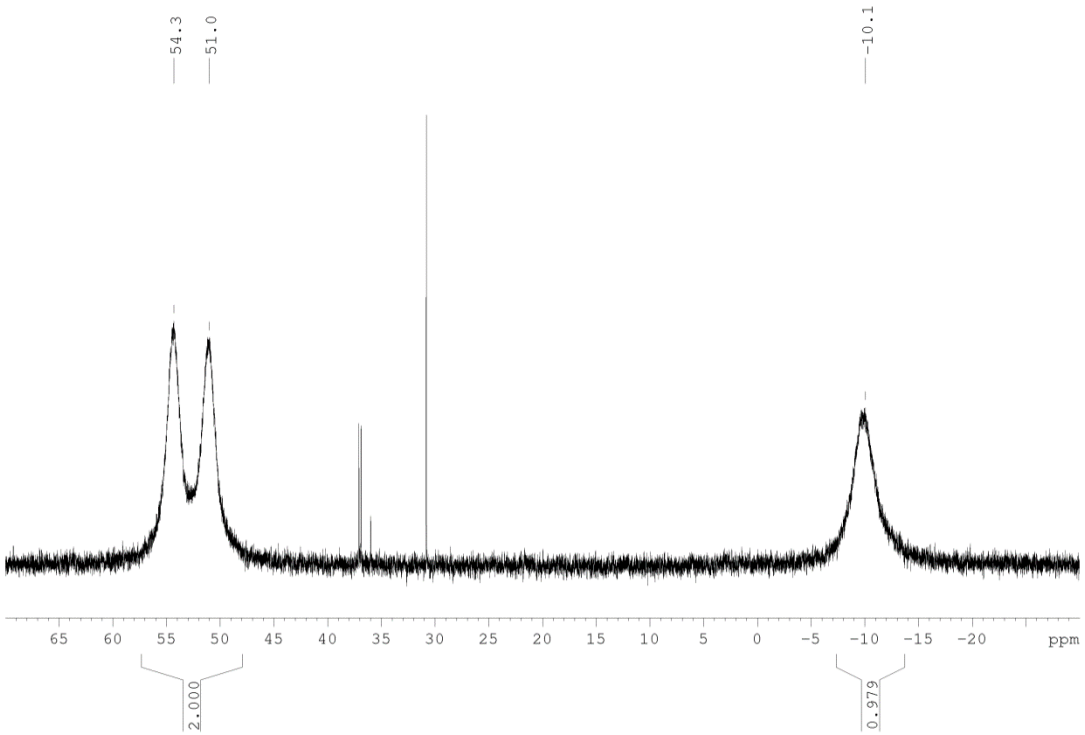

Figure S25. $^{31}P\{^{1}H\}$ NMR spectrum (C_6D_6, 298 K) for **11-Me**.

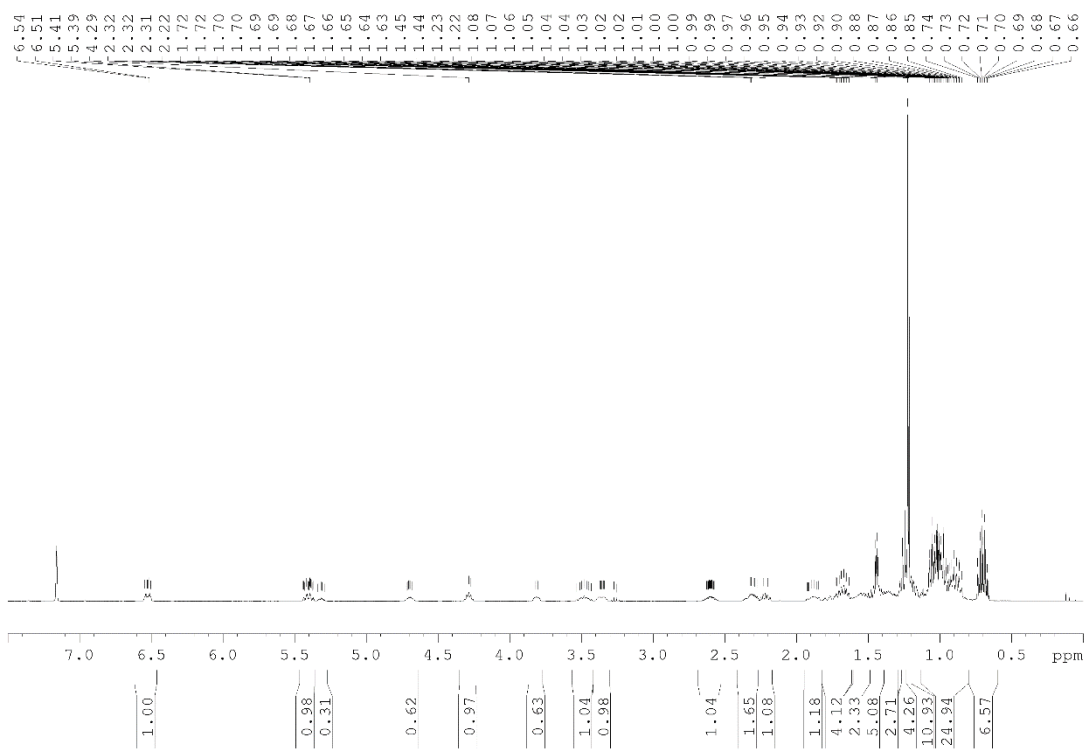

Figure S26. ^{1}H NMR spectrum (C_6D_6, 298 K) for **11-Et**.

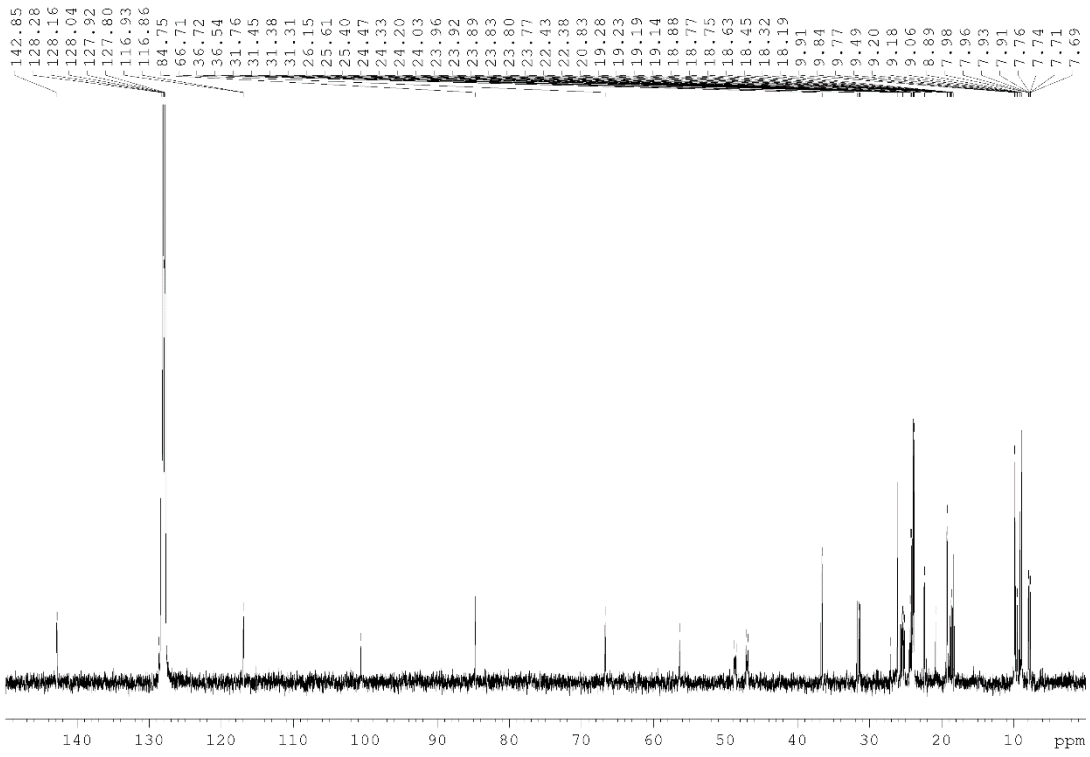

Figure S27. $^{13}C\{^{1}H\}$ NMR spectrum (C_6D_6, 298 K) for **11-Et**.

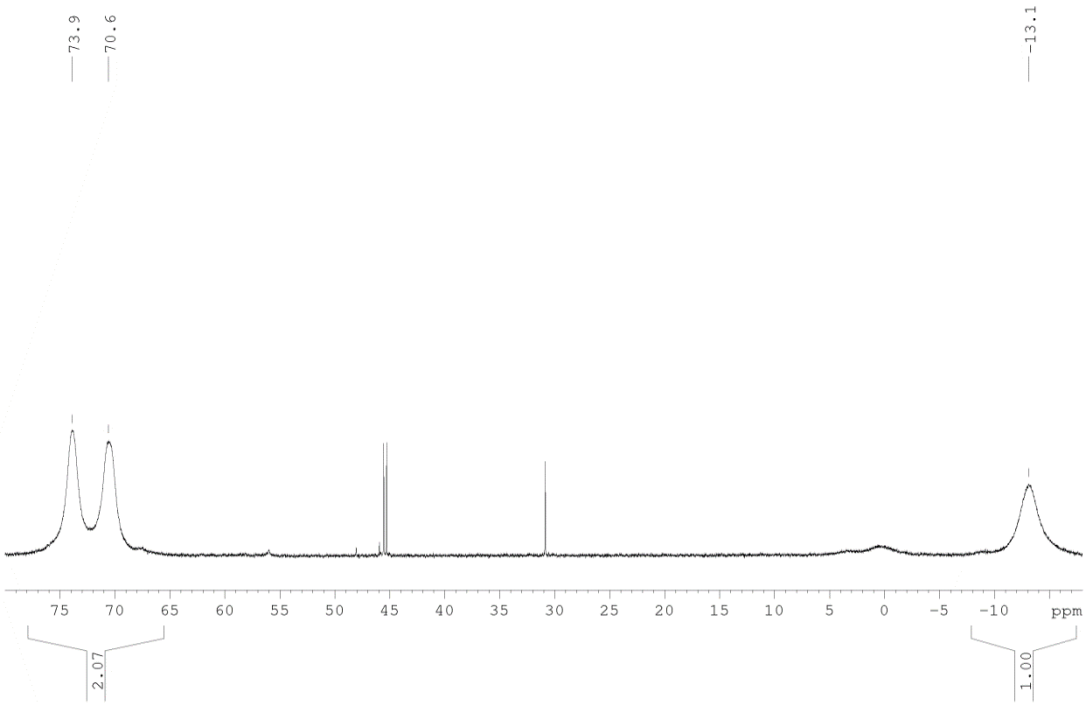

Figure S28. $^{31}P\{^{1}H\}$ NMR spectrum (C_6D_6, 298 K) for **11-Et**.

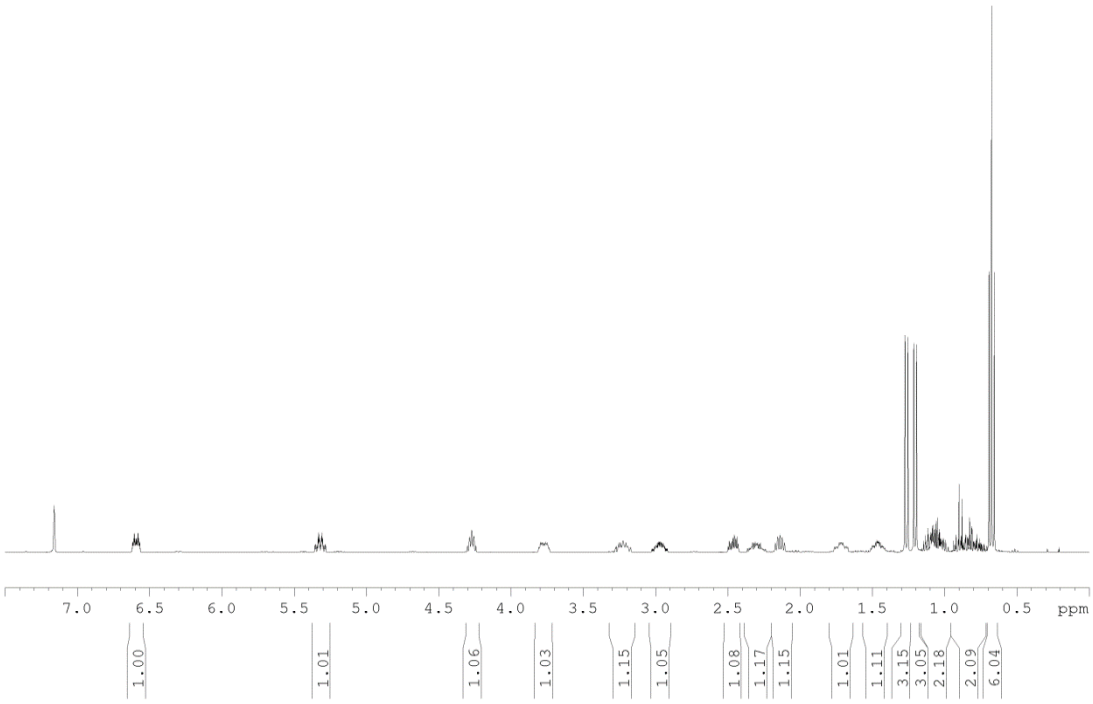

Figure S29. ^{1}H NMR spectrum (C_6D_6, 298 K) for **12-Me**.

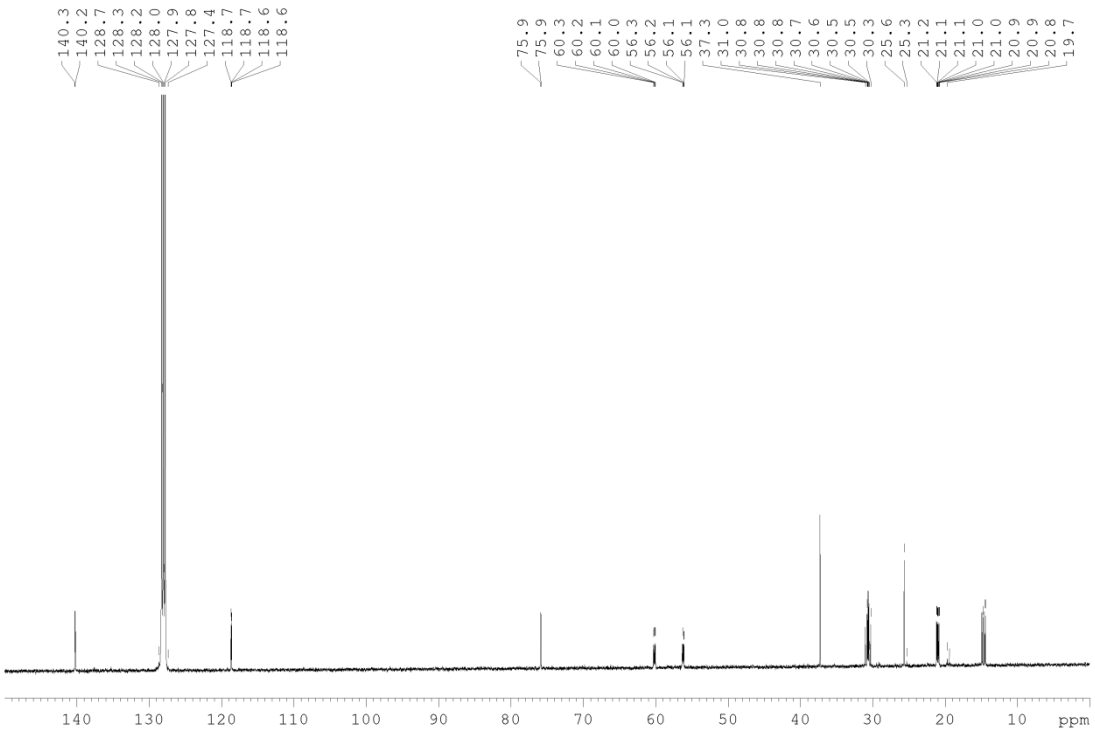

Figure S30. $^{13}C\{^{1}H\}$ NMR spectrum (C_6D_6, 298 K) for **12-Me**.

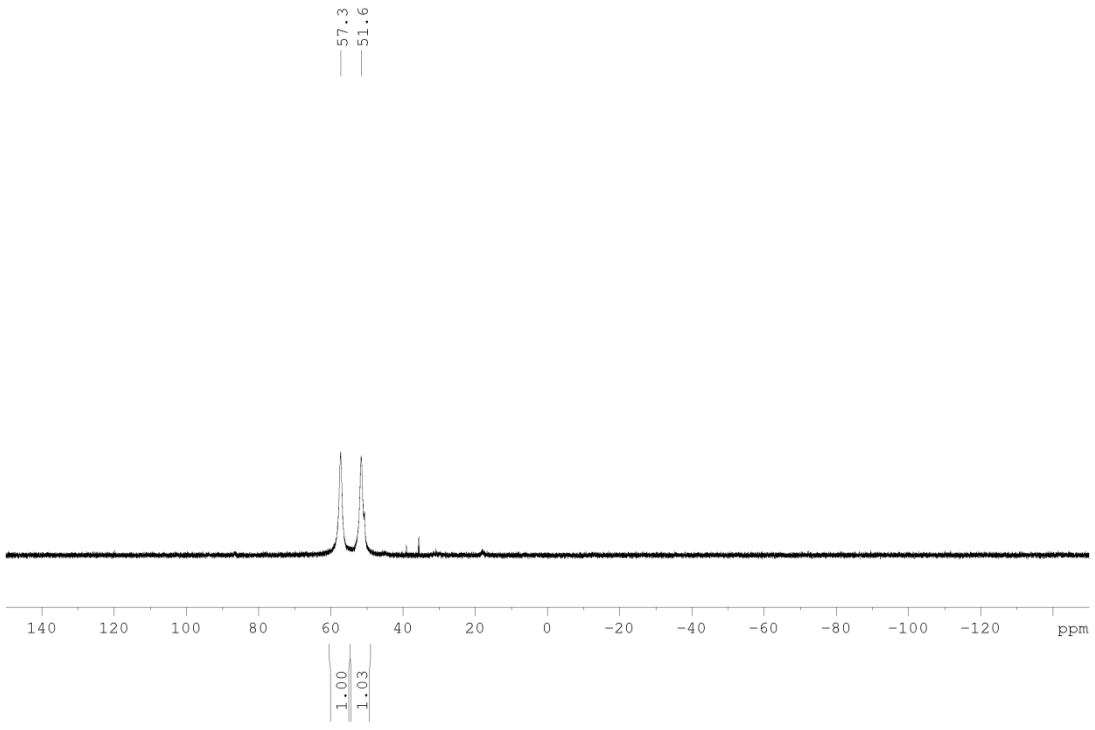

Figure S31. $^{31}P\{^{1}H\}$ NMR (C_6D_6, 298 K) spectrum for **12-Me**.

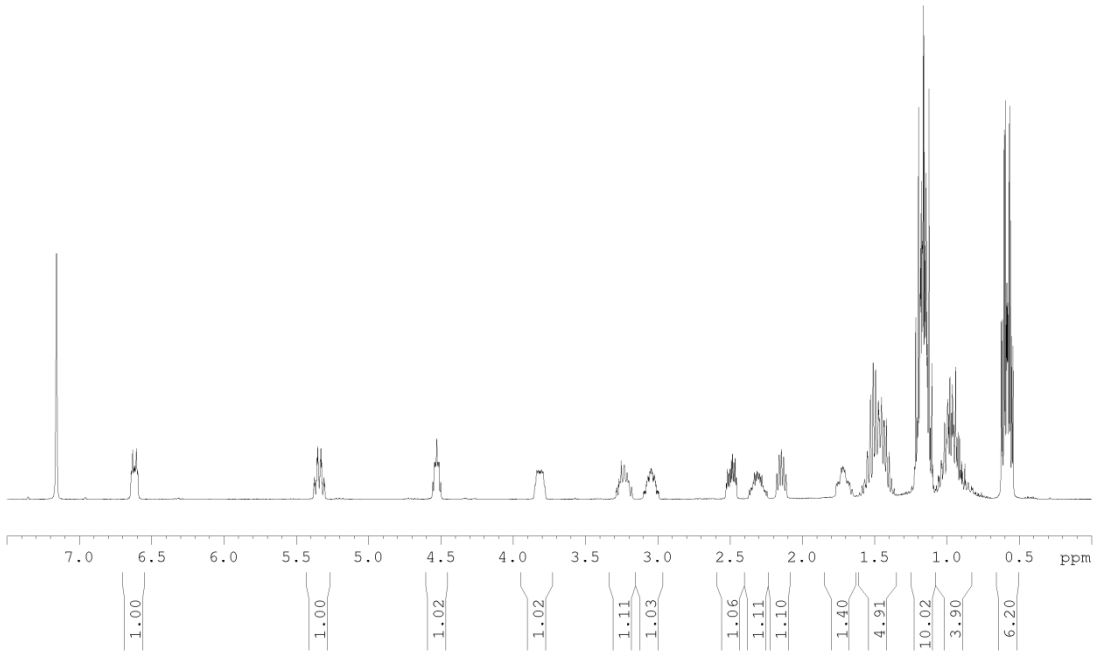

Figure S32. ^{1}H NMR spectrum (C_6D_6, 298 K) for **12-Et**.

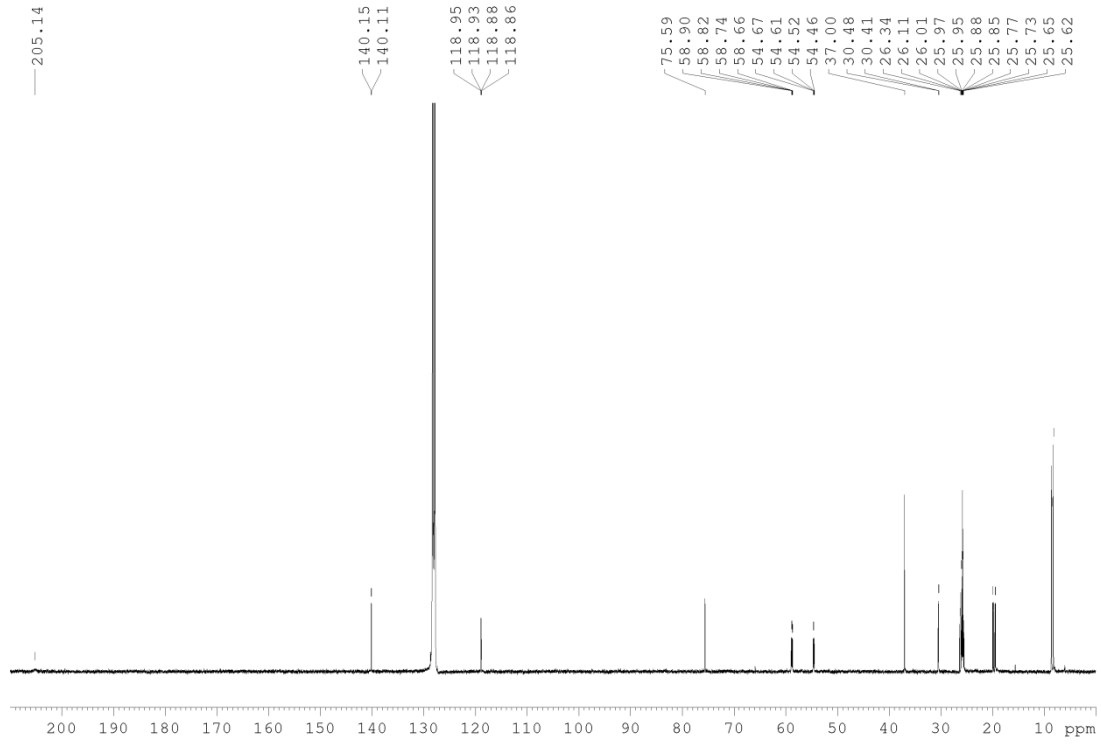

Figure S33. ^{13}C{^{1}H} NMR (C_6D_6, 298 K) spectrum for **12-Et**.

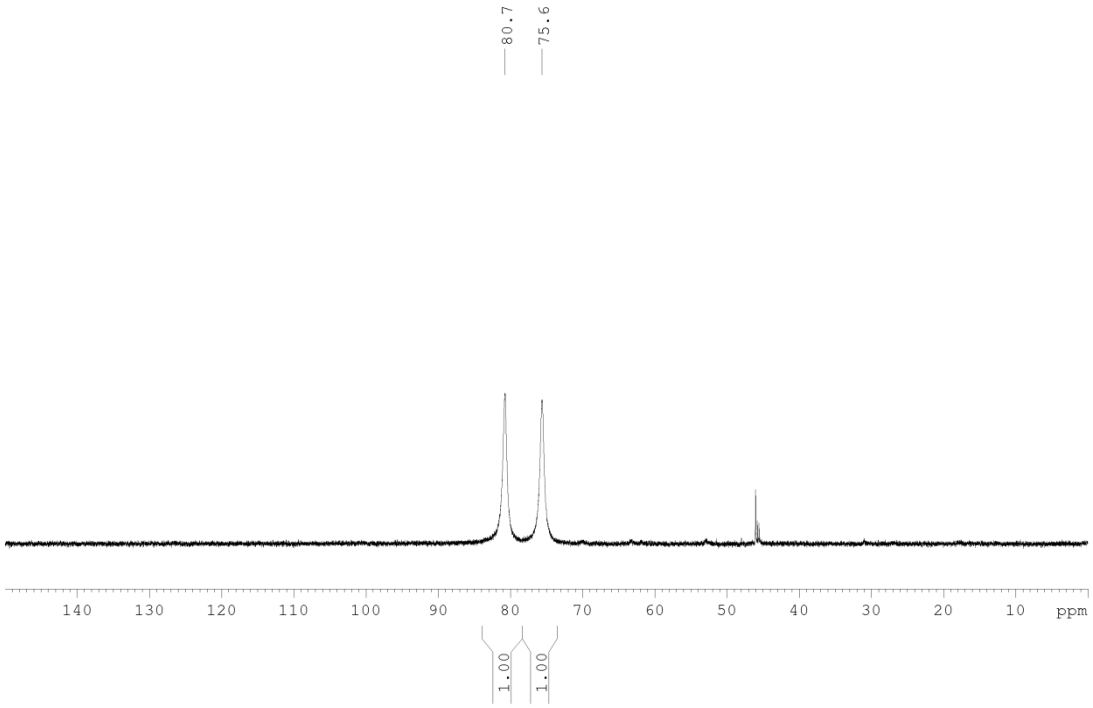

Figure S34. $^{31}P\{^{1}H\}$ NMR (C_6D_6, 298 K) spectrum for **12-Et**.

3. Computational Details

All calculations employed the B3LYP[17] functional and were carried out with Gaussian 09.[18] No symmetry restrictions were imposed (C1). C, H, and Co were represented by an all-electron 6-311G(d,p) basis set. The nature of extrema (minima) was established with analytical frequency calculations. The zero-point vibration energy (ZPE) and entropic contributions were estimated within the harmonic potential approximation (Table S2).

Table S2. Energies[a] of the optimized structures

Compound	E(0 K)[b] [Ha]	H(298 K)[c] [Ha]	G(298 K)[c] [Ha]
	B3LYP:		
[PdI'$_2$Co] (*S* = 1/2)	-2400.756094 (0.0)	-2400.720142 (0.0)	-2400.820962 (0.0)
[PdI'$_2$Co] (*S* = 3/2)	-2400.781113 (15.7)	-2400.746013 (16.2)	-2400.845037 (15.1)

[a]Values (in kcal/mol) given in parentheses refer to the energy difference to the lowest computed spin-configuration for the individual compounds. [b]DFT energy incl. ZPE. [c]Standard conditions T = 298.15 K and *p* = 1 atm.

4. Solid-state Magnetic Susceptibility Measurements

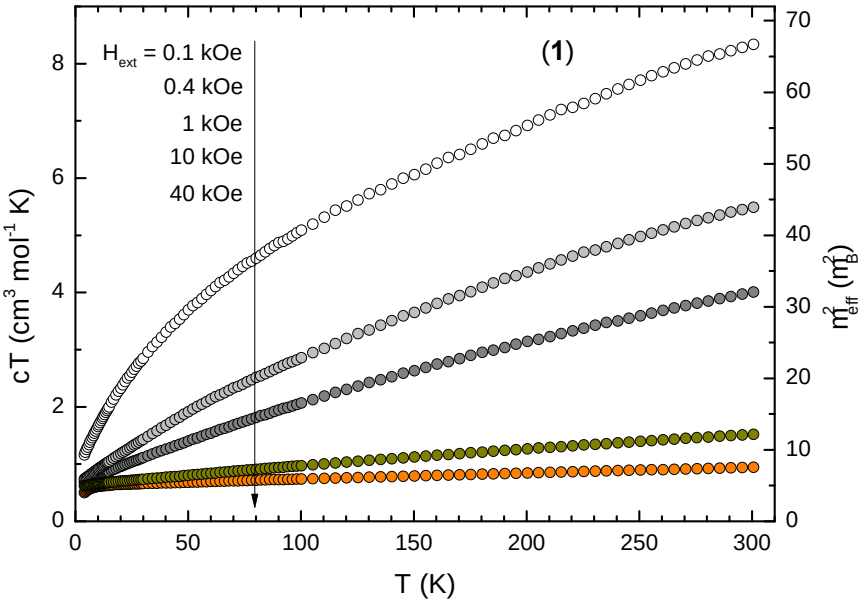

Figure S35. Magnetic susceptibility (χT) and effective magnetic moment (μ_{eff}^2) vs. T plot for complex **1**, recorded between T = 4 and 300 K with externally applied magnetic fields between H_{ext} = 0.1 and 40 kOe, respectively. Symbols: Experimental data.

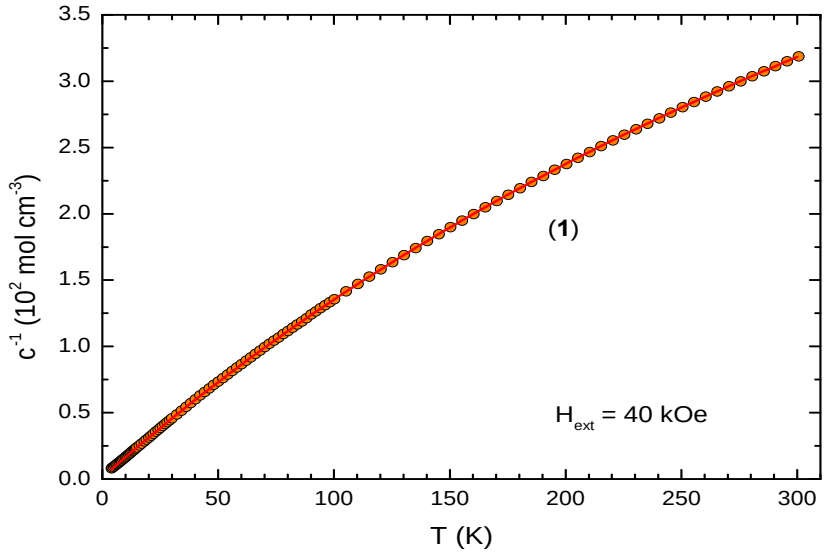

Figure S36. Inverse magnetic susceptibility (χ^{-1}) vs. T plot for complex **1**, recorded between T = 4 and 300 K with an externally applied magnetic field of H_{ext} = 40 kOe. Symbols: Experimental data. Line: Fit with a modified Curie-Weiss model described in the main text (parameters of the fit: C = 0.6445(4) cm^3 mol^{-1} K, θ = -0.83(2) K, χ_{TIP} = 10.0(1) × 10^{-4} cm^3 mol^{-1}).

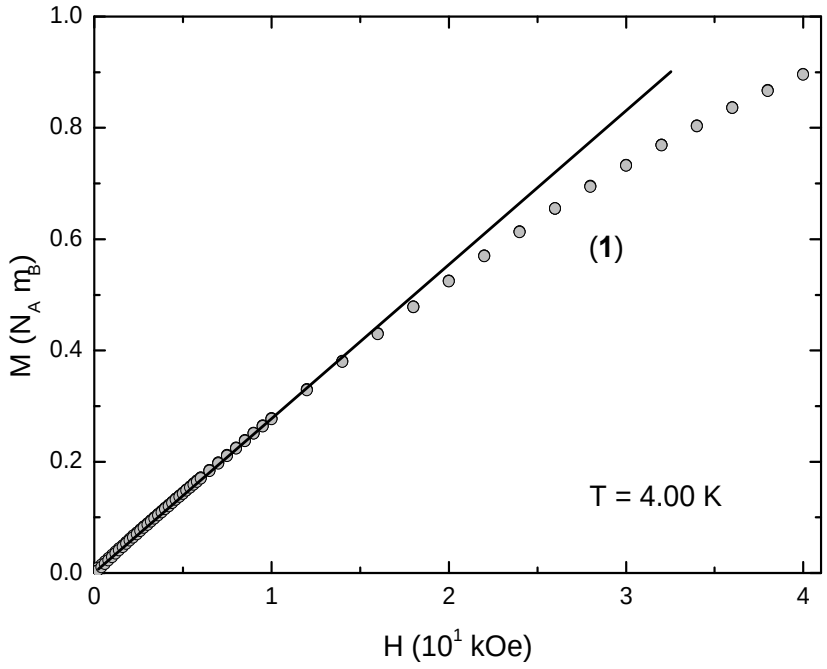

Figure S37. Isothermal magnetization (M) vs. magnetic field (H) plot for complex **1**, recorded at T = 4 K with externally applied magnetic fields between H_{ext} = 0.02 and 40 kOe. Symbols: Experimental data. The line represents the linear M(H) progression as expected for the Curie-Weiss approximation.

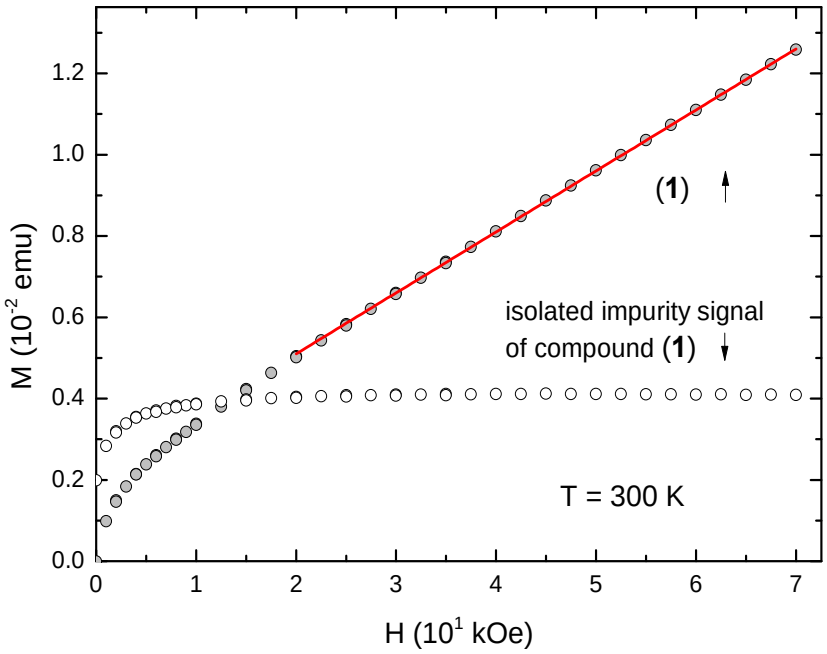

Figure S38. Isothermal magnetization (M) vs. magnetic field (H) plot for compound **1**, recorded at T = 300 K with externally applied magnetic fields between H_{ext} = 0.1 and 70 kOe. Symbols (grey): Experimental data. Line: Linear fit (for H > 20 kOe) of the M(H) data (parameters of the fit: M(0) = 2.1(1) × 10^{-3} emu, $\partial M/\partial H = \chi$ = 1.5(1) × 10^{-4} emu kOe^{-1}). This contribution is associated with the intrinsic paramagnetic susceptibility of complex **1**. Consistently, the determined magnetic susceptibility of χ = 1.5(1) × 10^{-4} emu kOe^{-1} corresponds to an effective magnetic moment of μ_{eff} = 2.19 μ_B, which is close to the value of $\mu_{eff} = \sqrt{8C}$ = 2.27 μ_B evaluated with the Curie-Weiss law approximation (cf., Figure

S36). Symbols (white): Experimental data after subtraction of the magnetization data attributed to complex **1** (red line). The remaining magnetization is ascribed to a small (ferromagnetic) impurity, presumably Co metal (see main text).

Comments concerning the analysis shown in Figure S38. The non-linear field dependence of the magnetization at low magnetic fields (i.e., below approx. H = 20 kOe) shown in Figure S38, in combination with the strong field dependence observed for the effective magnetic moment depicted in Figure S35, suggest the presence of (at least) two main contributions to the total magnetic susceptibility: (1) an intrinsic paramagnetic contribution attributed to complex **1,** which is reflected in the linear M(H) progression (red line, Figure S38) consistent with the Curie law approximation (i.e., $\chi = \partial M/\partial H = M/H$, independent of H), and (2) a contribution caused by a ferromagnetic impurity, which contributes to the total magnetic susceptibility predominantly at low external magnetic fields (i.e., when $\chi = \partial M/\partial H$ is large and strongly dependent on H). When the saturation magnetization of this component is reached (i.e., at approx. H_{ext} = 30 kOe), its contribution to the overall "paramagnetic" susceptibility is approx. $\chi = \partial M/\partial H = 0$.

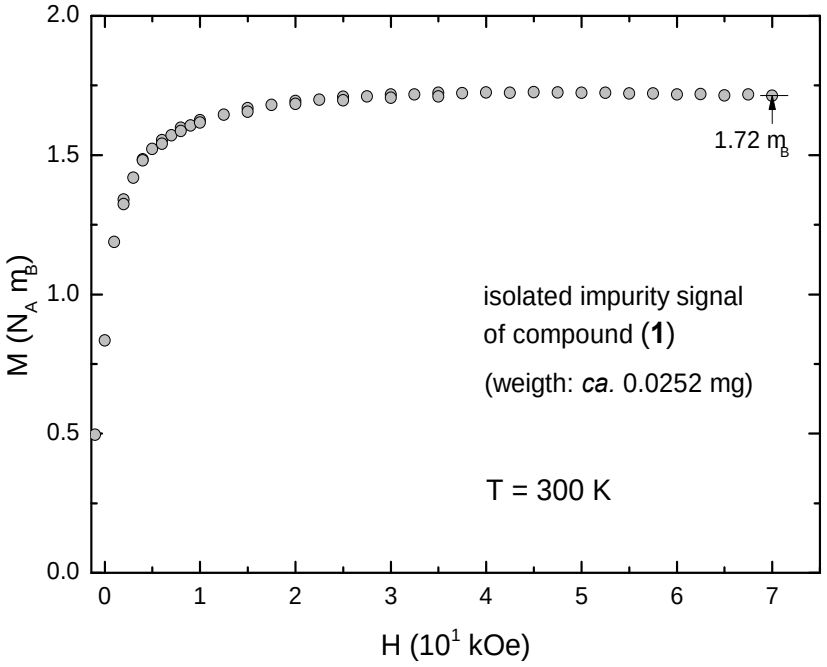

Figure S39. Isothermal magnetization (M) vs. magnetic field (H) plot for the isolated ferromagnetic Co impurity of compound **1**, recorded at T = 300 K with externally applied magnetic fields between H_{ext} = 0.1 and 70 kOe. Symbols: Experimental data taken from the measurement shown in Figure S38 after subtraction of the paramagnetic contributions to the magnetization associated with complex **1** (cf., white symbols in Figure S38). The calculated magnetization values shown in this figure (Figure S39) refer to the saturation magnetization expected for Co metal of ca. 1.72 μ_B.[2] With this assumption, the weight of the Co metal impurity was estimated to be *ca.* 0.0252 mg (for comparison: the total weight of the sample used for the measurement was 31.4 mg).

5. References

1. Spek, A. L. *Acta Cryst*. **2009**, *D65*, 148-155

2. Kittel, C., *Einführung in die Festkörperphysik*. R. Oldenbourg Verlag: München, 1996.